catalysts

MDPI

Article

Ab Initio Investigation of the Adsorption and Dissociation of O_2 on Cu-Skin $Cu_3Au(111)$ Surface

Yanlin Yu [1], Zhiming Liu [1], Wenxian Huang [2], Shan Zhou [1], Zuofu Hu [1] and Ligen Wang [3,*]

[1] School of Mathematics and Physics, Jinggangshan University, Ji'an 343009, China
[2] School of Architectural Engineering, Jinggangshan University, Ji'an 343009, China
[3] General Research Institute for Nonferrous Metals, Beijing 100088, China
* Correspondence: lg_wang1@yahoo.com; Tel.: +86-135-2113-4375; Fax: +86-10-82-240-096

Abstract: Surface adsorption and dissociation processes can have a decisive impact on the catalytic properties of metal alloys. We have used density functional theory to investigate the adsorption and dissociation of O_2 on Cu-skin $Cu_3Au(111)$ surface. The calculated results show that the b-f(h)-b adsorption configuration is the most energetically favorable on the Cu-skin $Cu_3Au(111)$ surface. For O_2 dissociation, there are two thermodynamically favorable dissociation paths. One path is from b-f-b to two O atoms in hcp sites, and the other path is from b-h-b to two O atoms in fcc sites. Moreover, the stability of O_2 adsorption is higher and the dissociation energy barrier of the adsorbed O_2 is lower as compared to those on the Cu(111) surface. This theoretical work provides valuable guidance for the practical application of Cu-Au alloys as highly efficient CO oxidation catalysts.

Keywords: adsorption; dissociation; density-functional theory calculations; Cu-skin $Cu_3Au(111)$ surface

Citation: Yu, Y.; Liu, Z.; Huang, W.; Zhou, S.; Hu, Z.; Wang, L. Ab Initio Investigation of the Adsorption and Dissociation of O_2 on Cu-Skin $Cu_3Au(111)$ Surface. *Catalysts* **2022**, *12*, 1407. https://doi.org/10.3390/catal12111407

Academic Editors: Yongjun Ji, Liwen Xing and Ke Wu

Received: 29 September 2022
Accepted: 1 November 2022
Published: 10 November 2022

1. Introduction

Bimetal alloys exhibit promising applications in various technologies related to surface science and heterogeneous catalysis [1–3]. In particular, they are significant in dominating catalytic reactions, such as selective hydrogenation [4], oxygen reduction [5], synthesis gas reaction [6], and synthesis of vinyl acetate [7]. This is attributed to their specific surface electronic properties affecting the surface adsorption and dissociation processes. Many theoretical studies have shown that the reaction process can have a decisive impact on catalytic performance. For example, Feng et al. [8] surveyed the electronic structures of cobalt-molybdenum bimetallic, arguing that H_2 adsorption/dissociation on the alloy surface was a key process determining the catalytic activity. Shin et al. [9] investigated the catalytic properties of Ag-Cu binary alloy in oxygen reduction reactions, and further confirmed that the activation energy of O_2 dissociation was a rate-determining process in the catalytic reaction. The study by Liu et al. [10] demonstrated that O_2 adsorption and dissociation on the surface of Cu-Au alloys were considered to be key processes to limit the rate of CO oxidation. Therefore, studying the reaction process will provide a significant support for understanding the catalytic reaction mechanism of binary catalysts.

Among the bimetallic systems, copper alloys have received much attention because of their wide application in a large number of chemical reactions including heterogeneous methanol reforming [11], methanol synthesis [12], the synthesis of diamond [13], and the reduction of 4-nitrophenol [14]. In the context of the CO oxidation reaction, the experiments have demonstrated that the Cu alloying with Au element could improve the efficiency of the CO oxidation reaction and promote the reaction toward desired products [15]. This is attributed to the synergistic interaction between Cu and Au, which improves the catalytic performance of the alloy. Although some studies [10,16,17] have indicated that the adsorption and dissociation of O_2 were the key processes to limit the rate of CO oxidation on the surface of noble metal catalysts, few studies have been carried out on the adsorption and

dissociation of O_2 on the surface of Cu-Au catalysts. Obviously, the theoretical calculations can provide necessary help for understanding the reaction processes.

In this work, we perform first-principles calculations to investigate the adsorption and dissociation of O_2 on the Cu-skin $Cu_3Au(111)$ surface. The calculated results show that the b-f(h)-b adsorption configuration is the most energetically favorable on the Cu-skin $Cu_3Au(111)$ surface. For O_2 dissociation, there are two thermodynamically favorable dissociation paths. One path is from b-f-b to two O atoms in hcp sites, and the other path is from b-h-b to two O atoms in fcc sites. Moreover, the stability of O_2 adsorption is higher and the dissociation energy barrier of the adsorbed O_2 is lower as compared to those on the Cu(111) surface. The remainder of the paper is organized as follows. In Section 2, the computational details are described. Section 3 presents the calculated results and discussion. A brief summary is given in Section 4.

2. Computational Methods

The spin-polarized DFT calculations were performed employing the Vienna Ab-initio Simulation Program (VASP) [18–20]. We used the projector augmented-wave method (PAW) [21,22] and the Perdew–Burke–Ernzerhof formulation of the generalized-gradient approximation (GGA-PBE) for the exchange correlation functional [23]. The plane-wave cutoff energy was set at 400 eV. The convergence criterion for the electronic self-consistent cycle was fixed to 10^{-5} eV per supercell and the ionic relaxation loop were set to 0.02 eV/Å. The electric dipole was neglected, and the Brillouin zone was sampled with a $5 \times 5 \times 1$ Monkhorst-Pack [24] k-point mesh for the slab calculations.

In this work, we chose low index (111) surface to simulate the surfaces of pure Cu and CuAu alloy system, mainly because the (111) surface may be the dominant facet [25]. The previous studies have shown that Cu_3Au alloys with $L1_2$ crystal structure can be widely used in various chemical reactions [26–28]. In addition, the catalyst inevitably contacts with air in the process of preparation and practical application, which will lead to oxygen adsorption-induced segregation, forming a copper segregation structure with 100% copper in the topmost surface layer and 50% copper in the second surface layer, which is the so-called Cu-skin structure [28]. Therefore, we employed the Cu-skin $Cu_3Au(111)$ alloys to investigate the adsorption and dissociation of O_2 on the surface of Cu-Au catalysts. The DFT-lattice constants for Cu_3Au and pure Cu were 3.79 and 3.63 Å, respectively, which are consistent with previously reported results [26,29]. Figure 1 shows the slab models for pure Cu(111) and $Cu_3Au(111)$ surfaces. We employed a 2×2 (111) unit cell for both slab models, which consisted of four atomic layers and six equivalent layers of vacuum. In all slab models, atoms in the top two layers were allowed to relax to the most stable configuration, while atoms in the bottom two layers were fixed to their bulk positions. Adsorbates were adsorbed on the surface of the model.

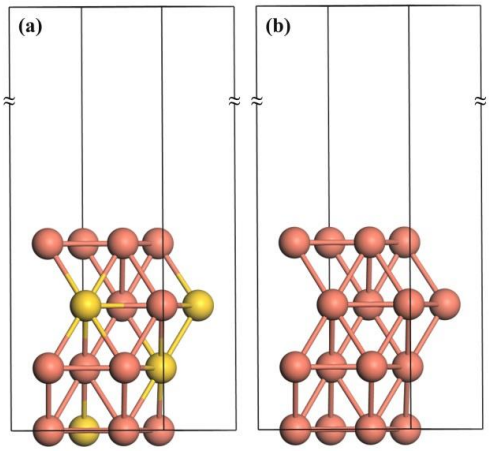

Figure 1. The slab models consist of (**a**) Cu-skin $Cu_3Au(111)$ surface, (**b**) pure Cu(111) surface. In the figure, brick-red and gold balls represent Cu and Au atoms, respectively.

The adsorption energies (E_{ads}) of molecular O_2 adsorbed on the pure Cu(111) and Cu-skin Cu_3Au(111) surfaces were calculated as following:

$$E_{ads,O_2} = E_{O_2-slab} - E_{slab} - E_{O_2} \quad (1)$$

In the equation, the first and second terms on the right-hand side correspond to the energies of substrates with and without O_2 adsorption, respectively, and the remaining term corresponds to the energy of the O_2 molecule. A negative value of E_{ads} indicates that it favors the adsorption of O_2 on the metal surface.

The transition states and minimum energy path (MEP) for O_2 dissociation on the Cu(111) and Cu-skin Cu_3Au(111) surfaces was studied by using the climbing-image nudged elastic band (CI-NEB) method [30,31]. The CI-NEB is a small modification of the NEB method, where the highest energy image is driven to the saddle point (transition state) in an attempt to maximize its energy along the band and minimize it in all other directions. When the algorithm converges, the highest energy images will be at an exact saddle point, so the CI-NEB method is currently the predominant method for finding the transition state and the minimum energy path between known reactants and products. Once a minimum energy path is determined, the transition state is located and the activation energy will be calculated as following:

$$E_a = E_b^{TS} - E_b^{PS} \quad (2)$$

In the equation, the E_b^{TS} corresponds to the total energy of the transition state and the E_b^{PS} corresponds to the total energy of the precursor state. The basis set superposition errors correction for the precursor state in our calculation was ignored because it had little effect on the calculated results.

3. Theoretical Results

3.1. The Adsorption of O_2

For Cu-skin Cu_3Au(111) surface, there are two kinds of nonequivalent Cu atoms in the topmost layer of the alloy because of the uneven distribution of Cu and Au atoms in the second layer. These two Cu atoms are denoted as Cu_1 and Cu_2, respectively, as shown in Figure 2a. For the Cu_1 atom, it is located at the center of one Au atom and two Cu atoms in the second layer of the surface; while for the Cu_2 atom, it is located at the center of one Cu atom and two Au atoms in the second layer of the surface. We can find that the Cu_1 atom is about 0.082 Å lower than the Cu_2 atom in the vertical position after the surface structure is relaxed. In addition, the Bader [32] analysis shows that Au in the alloy obtains fewer electrons from Cu_1 than from Cu_2, and the number of electrons is 0.04 and 0.07, respectively. This may be because the amount of Au close to Cu_1 is smaller than that of Au close to Cu_2. The similar phenomena can also be found in the Pt-skin Pt_3Fe [33] and Pt-skin Pt_3Cr [34] systems.

Many studies have shown that five types of stable adsorption sites for O_2 existed on the low-index (111) surface of transition metals, namely, b-f-b, t-f-b, b-h-b, t-h-b, and t-b-t sites [35]. For Cu-skin CuAu(111) surface, due to the presence of two nonequivalent Cu atoms in the topmost layer of the alloy, there are mainly two different adsorption configurations for each type of adsorption site. We calculated the adsorption energies of O_2 on these adsorption sites of Cu(111) and Cu-skin Cu_3Au(111), and the stable adsorption configurations and calculated results are shown in Figure 2 and Table 1, respectively. For the Cu(111) surface, we can find that the adsorption energies of O_2 on the b-h-b and b-f-b sites are the highest, both of which are −0.76 eV. When O_2 is adsorbed at the t-h-b, t-f-b, and t-b-t sites, their adsorption energies are −0.71, −0.71, and −0.50 eV, respectively. This calculation result is consistent with the previous theoretical calculation result [25]. For the Cu-skin Cu_3Au(111) surface, the adsorption energies at each adsorption site are very close, and they range from −1.07 to −1.15 eV. Similar to the Cu(111) surface, b-f-b1 and b-h-b1 are the two most stable adsorption configurations with values of −1.14 and −1.15 eV, respectively. In contrast to the Cu(111) surface, the t-b-t adsorption configuration is not

stable on the Cu-skin $Cu_3Au(111)$ surface. This may be due to the weak interaction between O_2 and the substrate [36]. The Bader analysis shows that the adsorption of O_2 will cause the Cu on the surface to lose more electrons. A part of these electrons is acquired by Au atoms in the second layer, and the other part is acquired by O_2 adsorbed on the surface. Furthermore, O_2 gains more electrons from the Cu-skin $Cu_3Au(111)$ surface than from the Cu(111) surface, suggesting that the modification of the surface electronic structure by alloying promotes the formation of strong adsorption bonds between O_2 and Cu atoms on the alloy surface.

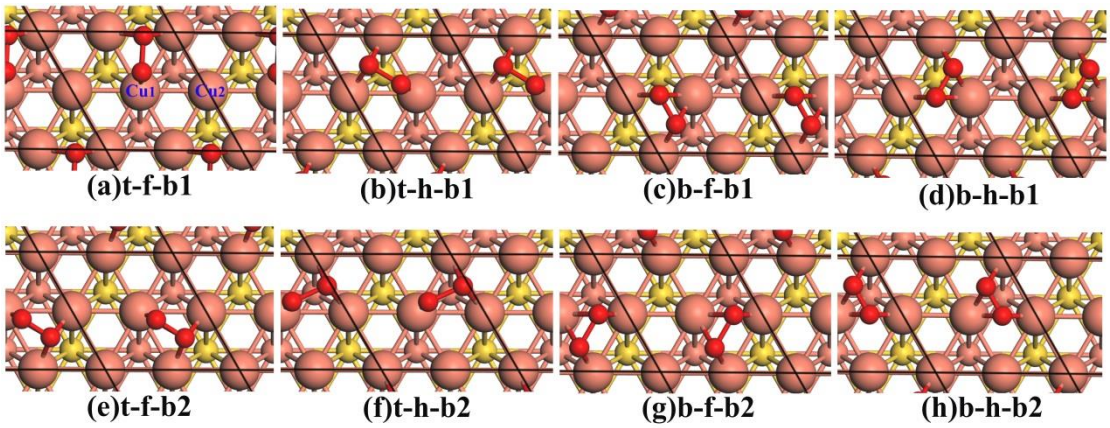

Figure 2. The top view for optimized configurations of O_2 adsorption on Cu-skin $Cu_3Au(111)$ surface. The two kinds of nonequivalent Cu atoms (Cu_1 and Cu_2) are marked in Figure 2a. The brick-red, gold, and red balls represent copper, gold, and oxygen atoms, respectively. For clarity, the topmost atoms on the surface are displayed with the biggest balls and only the top two layers are displayed.

Table 1. The adsorption energy of O_2 (E_{ads} in eV) and the number of electrons obtained by O_2 from the surfaces of Cu-skin $Cu_3Au(111)$ and Cu(111).

$Cu_3Au(111)$			Cu(111)		
Site	**E_{ads}**	**N_{chg}**	**Site**	**E_{ads}**	**N_{chg}**
t-f-b1	−1.08	0.92	t-f-b	−0.71	0.87
t-f-b2	−1.08	0.93	t-h-b	−0.71	0.87
t-h-b1	−1.09	0.91	t-b-t	−0.50	0.70
t-h-b2	−1.07	0.92	b-f-b	−0.76	0.94
b-f-b1	−1.14	1.01	b-h-b	−0.76	0.94
b-f-b2	−1.12	1.00			
b-h-b1	−1.15	1.01			
b-h-b2	−1.11	1.00			

3.2. The Electronic Structure of Cu-Skin Cu_3Au Surface

The density of states (DOS) can provide key information for understanding the electronic structure and bonding properties of alloy compounds, especially when it comes to investigating the adsorption properties of metal alloy surfaces, the d-band DOS is an extremely significant reference [37,38]. Figure 3 shows the d-band DOS of the Cu atoms in the outermost layer of alloys and pure metals in the absence of adsorption. From the figure, we can find that compared with the d-band center for Cu on the Cu(111) surface, the d-band center for Cu on the Cu-skin Cu_3Au (111) alloy surface is closer to the Fermi level. This similar phenomenon can also be seen in Pt and Pd alloys [39,40]. This phenomenon is attributed to the overlapping of the d-electron density of states for Cu and Au atoms in the alloy, which leads to the re-hybridization of the d-band DOS for Cu, thus promoting the d-band center of copper in the alloy to move closer to the Fermi level [41]. On the basis of the adsorption model established by Hammer and Nørskov [37,38], it is shown that the adsorption strength of the adsorbate on the metal surface is closely related to the d-band

center. When the center of the d-band moves to the high-energy region, the adsorption strength is larger. Therefore, the adsorption strength of O_2 on the Cu-skin $Cu_3Au(111)$ surface should be greater than that on the Cu(111) surface. This result is consistent with our calculation above.

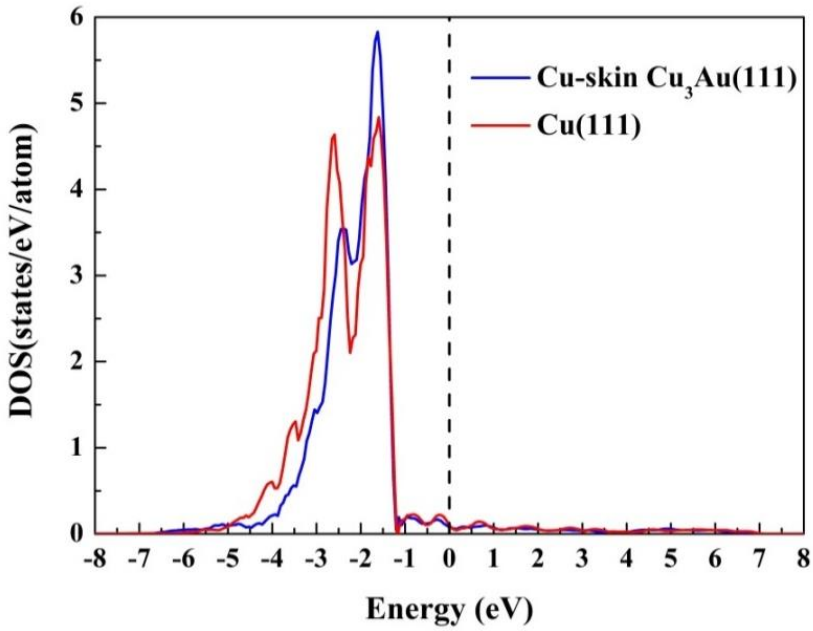

Figure 3. The calculated densities of states (DOS) of the Cu atoms in the Cu-skin $Cu_3Au(111)$ and Cu(111) surfaces. The d-band DOS of surface Cu atoms on Cu(111) is presented for comparison.

3.3. The Dissociation of O_2

Many studies have shown that studying the dissociation process of the adsorbate on the catalyst surface by using DFT calculations required knowledge of the initial and final states of the reaction [35,36,42–44]. According to the above calculation results, the oxygen molecule tends to be adsorbed on the b-f(h)-b sites. Therefore, we chose the b-f(h)-b adsorption configuration as the initial state of the reaction. Many studies [35,36,42,43] have also shown that it is impossible for two O atoms to simultaneously adsorb on a set of adjacent hcp and fcc sites after the O-O bond of the precursor is broken; this is because they will be very strongly repulsed, and the two O atoms are more inclined to adsorb on two adjacent hcp or two adjacent fcc sites. Therefore, there are two thermodynamically favorable dissociation paths for O_2 dissociation. One path is from b-f-b to 2×hcp (two O atoms adsorb on a set of adjacent hcp sites), and the other path is from b-h-b to 2×fcc (two O atoms adsorb on a set of adjacent fcc sites). For the $O_2/Cu_3Au(111)$ system, we only studied the dissociation process of the adsorption configurations of b-f-b1 and b-h-b1 with higher adsorption strength, and their dissociation processes are shown in Figure 4a,b, respectively. From the figure, we can find that the dissociation process of the adsorption configuration of b-f-b1 and b-h-b1 is very similar. Early in the dissociation process, they both form a transition state with a low energy barrier (less than 0.1 eV) by stretching the O-O bond. When the O-O bond is stretched to break, the two separated O atoms will be adsorbed on two adjacent stable adsorption sites. This shows that O_2 easily dissociates on the Cu-skin $Cu_3Au(111)$ surface and forms a stable adsorption structure, which is consistent with other theoretical studies [28,45].

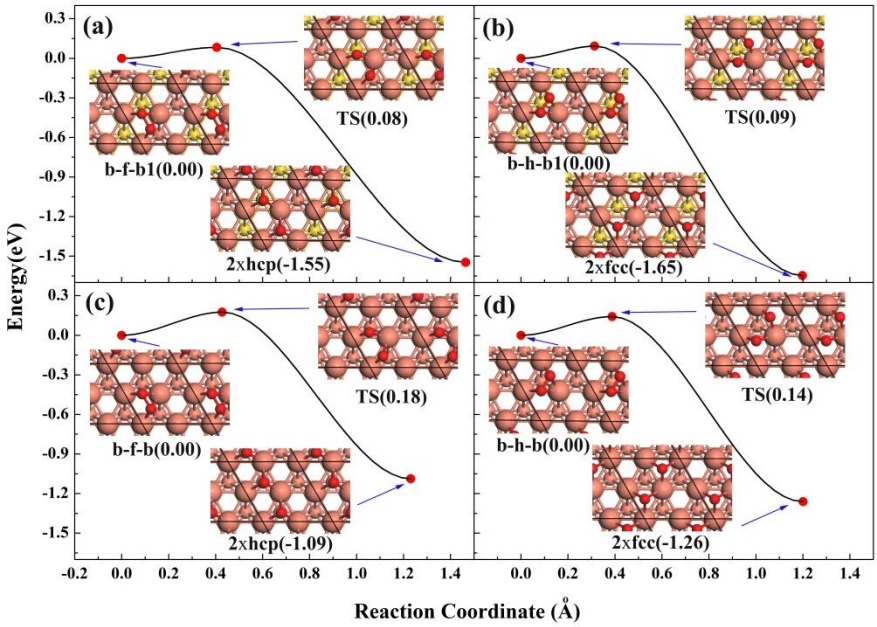

Figure 4. The minimum energy path (MEP) of the dissociation process for: (**a**) b-f-b1 adsorption state on Cu-skin $Cu_3Au(111)$ surface, (**b**) b-h-b1 adsorption state on Cu-skin $Cu_3Au(111)$ surface, (**c**) b-f-b adsorption state on Cu(111) surface, (**d**) b-h-b adsorption state on Cu(111) surface. The 2 × fcc (two O occupying a set of neighboring fcc sites) and 2 × hcp (two O occupying a set of neighboring hcp sites) are designated as the dissociation state of b-h-b and b-f-b adsorption configuration, respectively. TS represents the transitions state and the numbers in the brackets represent the energy of each state relative to initial state.

To further understand the dissociation process of O_2 on the Cu-skin $Cu_3Au(111)$ surface, we also investigated the dissociation process of the $O_2/Cu(111)$ system, and the results are shown in Figure 4c,d. It can be seen from the figure that although the dissociation process of the $O_2/Cu(111)$ system is very similar to that of the $O_2/Cu_3Au(111)$ system, the dissociation energy barrier of the $O_2/Cu(111)$ system is higher. For example, for the b-h-b and b-f-b states, their dissociation energy barriers are 0.14 and 0.18 eV, respectively, which are consistent with the estimate of 0.08–0.18 eV/O_2 by Habraken et al. [46]. This also explains why Cu alloying with the Au element can improve the efficiency of the CO oxidation reaction and promote the reaction toward desired products [15,47].

4. Conclusions

We have used density functional theory to investigate the adsorption and dissociation of O_2 on the Cu-skin $Cu_3Au(111)$ surface. The calculated results show that the b-f(h)-b adsorption configuration is the most energetically favorable on the Cu-skin $Cu_3Au(111)$ surface. For the Cu-skin $Cu_3Au(111)$ surface, the adsorption energies at each adsorption site are very close, and they range from −1.07 to −1.15 eV. In contrast to the Cu(111) surface, the t-b-t adsorption configuration is not stable on the Cu-skin $Cu_3Au(111)$ surface. This may be due to the weak interaction between O_2 and the substrate. The Bader analysis shows that O_2 gains more electrons from the Cu-skin $Cu_3Au(111)$ surface than from the Cu(111) surface, suggesting that the modification of the surface electronic structure by alloying promotes the formation of strong adsorption bonds between O_2 and Cu atoms on the alloy surface. For O_2 dissociation, there are two thermodynamically favorable dissociation paths. One path is from b-f-b to 2 × hcp (two O atoms adsorb on a set of adjacent hcp sites), and the other path is from b-h-b to 2 × fcc (two O atoms adsorb on a set of adjacent fcc sites). The dissociation energy barrier of O_2 on the Cu-skin $Cu_3Au(111)$ surface is lower as compared to those on the Cu(111) surface. This theoretical work provides valuable guidance for the practical application of Cu-Au alloys as highly efficient CO oxidation catalysts.

Author Contributions: Conceptualization, Y.Y. and L.W.; methodology, Y.Y.; software, Z.L.; validation, Z.L., S.Z. and Z.H.; formal analysis, S.Z.; investigation, W.H.; resources, Z.H.; data curation, W.H.; writing—original draft preparation, Y.Y.; writing—review and editing, Y.Y.; visualization, Z.L.; supervision, L.W.; project administration, L.W.; funding acquisition, Y.Y. All authors have read and agreed to the published version of the manuscript.

Funding: This research was funded by the Science and technology planning project of Jiangxi Provincial Department of Education, grant numbers GJJ180572 and GJJ160733, and the doctoral research project of Jinggangshan university, grant number JZB1815.

Data Availability Statement: Not applicable.

Conflicts of Interest: The authors declare no conflict of interest.

References

1. Stamenkovic, V.R.; Mun, B.S.; Arenz, M.; Mayrhofer, K.J.; Lucas, C.A.; Wang, G.; Ross, P.N.; Markovic, N.M. Trends in electrocatalysis on extended and nanoscale Pt-bimetallic alloy surfaces. *Nat. Mater.* **2007**, *6*, 241–247. [CrossRef] [PubMed]
2. Dong, Z.; Zhao, J.; Tian, Y.; Zhang, B.; Wu, Y. Preparation and performances of ZIF-67-derived FeCo bimetallic catalysts for CO_2 hydrogenation to light olefins. *Catalysts* **2020**, *10*, 455. [CrossRef]
3. Montemore, M.M.; van Spronsen, M.A.; Madix, R.J.; Friend, C.M. O_2 activation by metal surfaces: Implications for bonding and reactivity on heterogeneous catalysts. *Chem. Rev.* **2017**, *118*, 2816–2862. [CrossRef] [PubMed]
4. Murillo, L.E.; Goda, A.M.; Chen, J.G. Selective hydrogenation of the CO bond in acrolein through the architecture of bimetallic surface structures. *J. Am. Chem. Soc.* **2007**, *129*, 7101–7105. [CrossRef] [PubMed]
5. Tripkovic, V.; Hansen, H.A.; Rossmeisl, J.; Vegge, T. First principles investigation of the activity of thin film Pt, Pd and Au surface alloys for oxygen reduction. *Phys. Chem. Chem. Phys.* **2015**, *17*, 11647–11657. [CrossRef]
6. Pompeo, F.; Nichio, N.N.; Ferretti, O.A.; Resasco, D. Study of Ni catalysts on different supports to obtain synthesis gas. *Int. J. Hydrog. Energy* **2005**, *30*, 1399–1405. [CrossRef]
7. Chen, M.; Kumar, D.; Yi, C.-W.; Goodman, D.W. The promotional effect of gold in catalysis by palladium-gold. *Science* **2005**, *310*, 291–293. [CrossRef]
8. Feng, M.; Huang, J.; Peng, Y.; Huang, C.; Yue, X.; Huang, S. Tuning the electronic structures of cobalt-molybdenum bimetallic carbides to boost the hydrogen oxidation reaction in alkaline medium. *Chem. Eng. J.* **2022**, *428*, 131206. [CrossRef]
9. Shin, K.; Kim, D.H.; Lee, H.M. Catalytic characteristics of AgCu bimetallic nanoparticles in the oxygen reduction reaction. *ChemSusChem* **2013**, *6*, 1044–1049. [CrossRef]
10. Liu, X.; Wang, A.; Wang, X.; Mou, C.-Y.; Zhang, T. Au–Cu alloy nanoparticles confined in SBA-15 as a highly efficient catalyst for CO oxidation. *Chem. Commun.* **2008**, *27*, 3187–3189. [CrossRef]
11. Yong, S.T.; Ooi, C.W.; Chai, S.-P.; Wu, X. Review of methanol reforming-Cu-based catalysts, surface reaction mechanisms, and reaction schemes. *Int. J. Hydrog. Energy* **2013**, *38*, 9541–9552. [CrossRef]
12. Graciani, J.; Mudiyanselage, K.; Xu, F.; Baber, A.E.; Evans, J.; Senanayake, S.D.; Stacchiola, D.J.; Liu, P.; Hrbek, J.; Sanz, J.F. Highly active copper-ceria and copper-ceria-titania catalysts for methanol synthesis from CO_2. *Science* **2014**, *345*, 546–550. [CrossRef] [PubMed]
13. Chen, L.; Zhu, P.; Ma, H.; Jia, X.; Wakatsuki, M.; Zou, G. Effects of copper-based alloy on the synthesis of single-crystal diamond. *J. Phys. Condens. Matter* **2002**, *141*, 10957–10961. [CrossRef]
14. Menumerov, E.; Gilroy, K.D.; Hajfathalian, M.; Murphy, C.J.; Neretina, S. Plastically deformed Cu-based alloys as high-performance catalysts for the reduction of 4-nitrophenol. *Catal. Sci. Technol.* **2016**, *6*, 5737–5745. [CrossRef]
15. Bauer, J.C.; Mullins, D.; Li, M.; Wu, Z.; Payzant, E.A.; Overbury, S.H.; Dai, S. Synthesis of silica supported AuCu nanoparticle catalysts and the effects of pretreatment conditions for the CO oxidation reaction. *Phys. Chem. Chem. Phys.* **2011**, *13*, 2571–2581. [CrossRef]
16. Hashmi, A.S.K.; Hutchings, G.J. Gold catalysis. *Angew. Chem. Int. Ed.* **2006**, *45*, 7896–7936. [CrossRef]
17. Bond, G.C.; Thompson, D.T. Catalysis by gold. *Catal. Rev.-Sci. Eng.* **1999**, *41*, 319–388. [CrossRef]
18. Kresse, G.; Furthmüller, J. Efficiency of ab-initio total energy calculations for metals and semiconductors using a plane-wave basis set. *Comput. Mater. Sci.* **1996**, *6*, 15–50. [CrossRef]
19. Kresse, G.; Furthmüller, J. Efficient iterative schemes for ab initio total-energy calculations using a plane-wave basis set. *Phys. Rev. B Condens. Matter* **1996**, *54*, 11169–11186. [CrossRef]
20. Kresse, G.; Hafner, J. Ab initio molecular-dynamics simulation of the liquid-metal-amorphous-semiconductor transition in germanium. *Phys. Rev. B* **1993**, *49*, 14251–14269. [CrossRef]
21. Blöchl, P.E. Projector augmented-wave method. *Phys. Rev. B Condens. Matter* **1994**, *50*, 2665–2668. [CrossRef] [PubMed]
22. Kresse, G.; Joubert, D. From ultrasoft pseudopotentials to the projector augmented-wave method. *Phys. Rev. B* **1999**, *59*, 1758–1775. [CrossRef]
23. Perdew, J.P.; Burke, K.; Ernzerhof, M. Generalized Gradient Approximation Made Simple. *Phys. Rev. Lett.* **1996**, *77*, 3865–3868. [CrossRef] [PubMed]

24. Monkhorst, H.J.; Hendrik, J.; James, D. Special points for Brillouin-zone integrations. *Phys. Rev. B* **1976**, *13*, 5188–5192. [CrossRef]
25. Dhifallah, M.; Dhouib, A.; Aldulaijan, S.; Di Renzo, F.; Guesmi, H. First-principles study of Au–Cu alloy surface changes induced by gas adsorption of CO, NO, or O_2. *J. Chem. Phys.* **2016**, *145*, 024701. [CrossRef]
26. Hirunsit, P.; Soodsawang, W.; Limtrakul, J. CO_2 Electrochemical Reduction to Methane and Methanol on Copper-Based Alloys: Theoretical Insight. *J. Phys. Chem. C* **2015**, *119*, 8238–8249. [CrossRef]
27. Hirunsit, P. Electroreduction of Carbon Dioxide to Methane on Copper, Copper–Silver, and Copper–Gold Catalysts: A DFT Study. *J. Phys. Chem. C* **2013**, *117*, 8262–8268. [CrossRef]
28. Oka, K.; Tsuda, Y.; Makino, T.; Okada, M.; Hashinokuchi, M.; Yoshigoe, A.; Teraoka, Y.; Kasai, H. The effects of alloying and segregation for the reactivity and diffusion of oxygen on Cu_3Au (111). *Phys. Chem. Chem. Phys.* **2014**, *16*, 19702–19711. [CrossRef]
29. Yu, Y.; Huang, W.; Liu, Z.; Hu, Z.; Wang, L. First-principles study of surface segregation in bimetallic Cu_3M (1 1 1)(M = Au, Ag, and Zn) alloys in presence of adsorbed CO. *Comput. Mater. Sci.* **2022**, *212*, 111550. [CrossRef]
30. Henkelman, G.; Jónsson, H. Improved tangent estimate in the nudged elastic band method for finding minimum energy paths and saddle points. *J. Chem. Phys.* **2000**, *113*, 9978–9985. [CrossRef]
31. Henkelman, G.; Uberuaga, B.P.; Jónsson, H. A climbing image nudged elastic band method for finding saddle points and minimum energy paths. *J. Chem. Phys.* **2000**, *113*, 9901–9904. [CrossRef]
32. Henkelman, G.; Arnaldsson, A.; Jónsson, H. A fast and robust algorithm for Bader decomposition of charge density. *Comput. Mater. Sci.* **2006**, *36*, 354–360. [CrossRef]
33. Hirschl, R.; Delbecq, F.; Sautet, P.; Hafner, J. $Pt_{80}Fe_{20}$ surface from first principles: Electronic structure and adsorption of CO and atomic H. *Phys. Rev. B* **2002**, *66*, 155438. [CrossRef]
34. Anderson, A.B. Theory for the Potential Shift for OH ads Formation on the Pt Skin on Pt_3Cr (111) in Acid. *J. Electrochem. Soc.* **2004**, *151*, E85.
35. Xu, Y.; Mavrikakis, M. Adsorption and dissociation of O_2 on Cu (111): Thermochemistry, reaction barrier and the effect of strain. *Surf. Sci.* **2001**, *494*, 131–144. [CrossRef]
36. Yang, Z.; Wang, J.; Yu, X. The adsorption, diffusion and dissociation of O_2 on Pt-skin Pt_3Ni (111): A density functional theory study. *Chem. Phys. Lett.* **2010**, *499*, 83–88. [CrossRef]
37. Hammer, B.; Norskov, J.K. Why gold is the noblest of all the metals. *Nature* **1995**, *376*, 238–240. [CrossRef]
38. Hammer, B.; Nørskov, J.K. Electronic factors determining the reactivity of metal surfaces. *Surf. Sci.* **1995**, *343*, 211–220. [CrossRef]
39. Kitchin, J.; Nørskov, J.K.; Barteau, M.; Chen, J. Modification of the surface electronic and chemical properties of Pt (111) by subsurface 3d transition metals. *J. Chem. Phys.* **2004**, *120*, 10240–10246. [CrossRef]
40. Hensley, A.J.R.; Zhang, R.; Wang, Y.; Mcewen, J.S. Tailoring the Adsorption of Benzene on PdFe Surfaces: A Density Functional Theory Study. *J. Phys. Chem. C* **2013**, *117*, 24317–24328. [CrossRef]
41. Schweitzer, N.; Xin, H.; Nikolla, E.; Miller, J.T.; Linic, S. Establishing relationships between the geometric structure and chemical reactivity of alloy catalysts based on their measured electronic structure. *Top. Catal.* **2010**, *53*, 348–356. [CrossRef]
42. Yang, Z.; Wang, J.; Yu, X. Density functional theory studies on the adsorption, diffusion and dissociation of O_2 on Pt(111). *Phys. Lett. A* **2010**, *374*, 4713–4717. [CrossRef]
43. Xu, Y.; Ruban, A.V.; Mavrikakis, M. Adsorption and dissociation of O_2 on Pt−Co and Pt−Fe alloys. *J. Am. Chem. Soc.* **2004**, *126*, 4717–4725. [CrossRef] [PubMed]
44. Diao, Z.Y.; Han, L.L.; Wang, Z.X.; Dong, C.C. The adsorption and dissociation of O_2 on Cu low-index surfaces. *J. Phys. Chem. B* **2005**, *109*, 5739–5745. [CrossRef] [PubMed]
45. Okada, M.; Hashinokuchi, M.; Fukuoka, M.; Kasai, T.; Moritani, K.; Teraoka, Y. Protective layer formation during oxidation of Cu_3Au(100) using hyperthermal O_2 molecular beam. *Appl. Phys. Lett.* **2006**, *89*, 201912. [CrossRef]
46. Habraken, F.; Kieffer, E.P.; Bootsma, G. A study of the kinetics of the interactions of O_2 and N_2O with a Cu(111) surface and of the reaction of CO with adsorbed oxygen using AES, LEED and ellipsometry. *Surf. Sci.* **1979**, *83*, 45–59. [CrossRef]
47. Liu, Y.; Xu, C.; Cen, W.; Li, H. Design strategy of bifunctional catalysts for CO oxidation. *Fuel* **2022**, *320*, 123909. [CrossRef]